Out-of-Equilibrium Mechanical Disruption of β-Amyloid-Like Fibers using Light-Driven Molecular Motors

Dania Daou, Yohan Zarate, Mounir Maaloum, Dominique Collin, Guillaume Fleith, Doru Constantin, Emilie Moulin, Nicolas Giuseppone

▶ **To cite this version:**

Dania Daou, Yohan Zarate, Mounir Maaloum, Dominique Collin, Guillaume Fleith, et al.. Out-of-Equilibrium Mechanical Disruption of β-Amyloid-Like Fibers using Light-Driven Molecular Motors. Advanced Materials, 2024, 36 (18), pp.2311293. 10.1002/adma.202311293 . hal-04737459

HAL Id: hal-04737459
https://hal.science/hal-04737459v1

Submitted on 15 Oct 2024

HAL is a multi-disciplinary open access archive for the deposit and dissemination of scientific research documents, whether they are published or not. The documents may come from teaching and research institutions in France or abroad, or from public or private research centers.

L'archive ouverte pluridisciplinaire **HAL**, est destinée au dépôt et à la diffusion de documents scientifiques de niveau recherche, publiés ou non, émanant des établissements d'enseignement et de recherche français ou étrangers, des laboratoires publics ou privés.

Distributed under a Creative Commons Attribution - NonCommercial - NoDerivatives 4.0 International License

Out-of-equilibrium mechanical disruption of β-amyloid-like fibers using light-driven molecular motors

*Dania Daou,[a] Yohan Zarate,[a] Mounir Maaloum,[a] Dominique Collin,[b] Guillaume Fleith,[b] Doru Constantin,[b] Emilie Moulin,[a] and Nicolas Giuseppone[a,c]**

[a] D. Daou, Y. Zarate, Prof. Dr. M. Maaloum, Dr. E. Moulin and Prof. Dr. N. Giuseppone
SAMS Research Group, Université de Strasbourg, CNRS, Institut Charles Sadron UPR 22
67000 Strasbourg, France
E-mail: giuseppone@unistra.fr
[b] Dr. D. Collin, Dr. D. Constantin, G. Fleith
CNRS, Institut Charles Sadron UPR 22 67000 Strasbourg, France
[c] Institut Universitaire de France (IUF)

Keywords:

Responsive materials – Out-of-equilibrium systems – Hydrogels – β-amyloid structures – Molecular machines – Molecular motors

Abstract:

Artificial molecular motors have the potential to generate mechanical work on their environment by producing autonomous unidirectional motions when supplied with a source of energy. However, the harnessing of this mechanical work to subsequently activate various endoenergetic processes that can be useful in materials science remains elusive. Here we show that by integrating a light-driven rotary motor through hydrogen bonds in a β-amyloid-like structure forming supramolecular hydrogels, the mechanical work generated during the constant rotation of the molecular machine under UV irradiation is sufficient to disrupt the β-amyloid fibers and to trigger a gel-to-sol transition at macroscopic scale. This melting of the gel under UV irradiation occurs 25 °C below the temperature needed to melt it by solely using thermal activation. In the dark, a reversible sol-gel transition is observed as the system fully recovers its original microstructure, thus illustrating the possible access to new kinds of motorized materials that can be controlled by advanced out-of-equilibrium thermodynamics.

1. Introduction

Artificial molecular machines are made of subcomponents that can precisely move relative to one another, and produce useful mechanical actuations on their environment (*i.e.* modify the chemical or physical properties of a system).[1–7] Such molecular machines are commonly divided between two distinct categories: (*i*) Molecular switches, which are bistable (or multistable) species influencing their environment as a function of their isomerization state (*i.e.* in the simplest case a state A or a state B); and (*ii*) Molecular motors, which move their subcomponents along a nonreversible pathway and have the potential to influence a system as a function of their motion trajectory, independently of their configurational state.[8,9] When supplied with a constant source of external energy, a molecular motor can repeat a unidirectional motion autonomously and indefinitely by using various kinds of ratcheting mechanisms.[10–14] Therefore, as opposed to molecular switches, molecular motors are able to continuously and progressively increase the mechanical work they perform on their environment, as long as they cycle motion. So far, the implementation of molecular machines in material science has been quasi-exclusively the result of the integration of simple molecular switches, either in the form of configurational isomers or of bistable mechanical bonds,[9,15–17] and in some examples by taking advantage of the different (meta)stable states adopted by molecular motors.[18,19] For instance, a sol-gel transition was recently described by making use of the two-state *cis* (sol) ↔ *trans* (gel) isomerization of a light-driven molecular motor, therefore reminiscent of an elementary bistable switching system.[20] Conversely, examples of real molecular motors that can truly influence materials' properties because of their autonomous and continuous unidirectional motion (independently of their state) remain scarce.[21,22] However, this kind of approach is of particular fundamental and technological interests because it holds the potential to generate continuous mechanical work within a system, and therefore to access advanced responsive out-of-equilibrium materials displaying thermodynamic properties approaching those encountered in living systems.[23]

Following our recent works demonstrating the integration of light-driven rotary motors[24–26] across length scales in chemical gels,[21,27,28] we became interested in the possibility of making use of their unidirectional rotation in supramolecular polymers and polymer networks, in order to drive the internal perturbation of weak bonds by nanomechanical actuation. Therefore, we decided to integrate a light-driven rotary motor in a supramolecular (physical) hydrogel through reversible hydrogen bond motifs. In the literature, carboxylic acid and pyridine moieties are well-known to form efficient intermolecular hydrogen bonds.[29,30] For instance, this type of supramolecular interaction can be used with small peptides (*i*) to invert the supramolecular chirality of phenylalanine-based nanofibrous structures in hydrogels[31–33], (*ii*) to design different hierarchical self-assemblies forming multi-responsive gels[34], and (*iii*) to tune the amyloid-like secondary structures of supramolecular dipeptide co-self-assemblies.[35] In the present work, we exploit such a co-self-assembly approach by implementing carboxylic acids and pyridine moieties for the design of an entirely new type of motorized hydrogel, and with the objective of probing the effect of the motor rotation / torque on such a dynamic supramolecular system.

2. Results and Discussion

2.1. Co-self-assembly of motorized supramolecular hydrogels

The main supramolecular co-self-assembly of this study is composed of three components (**Figure 1a**): (*i*) a light-driven rotary motor functionalized with four carboxylic acids (motor tetra-acid, **MTA**); (*ii*) a carboxybenzyl-protected diphenylalanine (**Z-FF**); and (*iii*) a bipyridine (**BPY**) (see supplementary information (SI) for all synthetic protocols and products characterization).

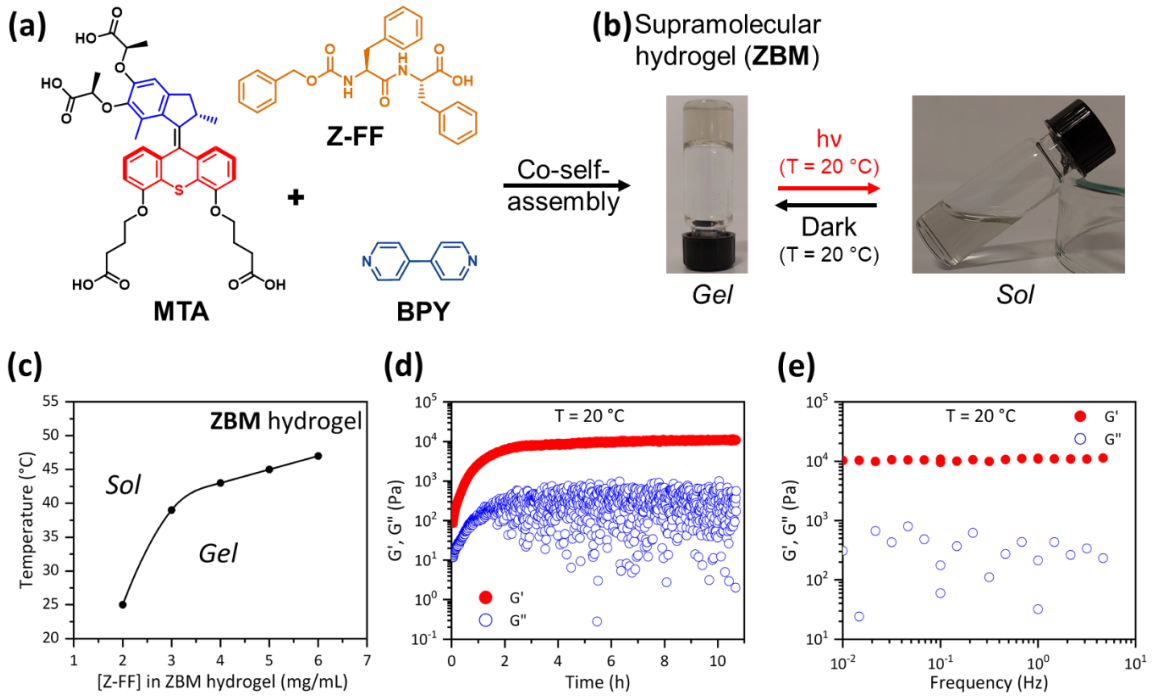

Figure 1. Chemical structures, apparent macroscopic behaviour, and rheology of ZBM hydrogels. (**a**) Chemical structures of motor tetra-acid (**MTA**), carboxybenzyl-protected diphenylalanine (**Z-FF**) and bipyridine (**BPY**), and their co-self-assembly in supramolecular **ZBM** hydrogel (5 mg/mL of **Z-FF**, molar ratio 4 **Z-FF**: 4 **BPY**: 1 **MTA**, 0.88% *wt*/*wt* in water, pH 5.7). (**b**) Irradiation of **ZBM** hydrogel with UV light (365 nm; 365 $mW.cm^{-2}$) for 20 minutes, at a constant temperature (T = 20 °C), resulting in gel-sol phase transition, followed by a sol-gel transition in the dark at the same temperature. (**c**) Temperature-concentration melting phase diagram of **ZBM** hydrogels (molar ratio 4: 4: 1) at pH 5.7; determined using the vial inversion method. (**d**) Time sweep rheology experiment of **ZBM** hydrogel during its formation (5 mg/mL of **Z-FF**, molar ratio 4: 4: 1), at constant temperature (20 °C), frequency (1 Hz) and stress (σ = 0.5 Pa). (**e**) Frequency sweep rheology experiment of **ZBM** hydrogel (5 mg/mL of **Z-FF**, molar ratio 4: 4: 1) at constant temperature (20 °C) and stress (σ = 0.5 Pa).

When a 4: 4: 1 molar ratio of **Z-FF**: **BPY**: **MTA** is mixed in water at a pH of 5.7, and at a concentration of 5 mg/mL for **Z-FF**, a self-supporting supramolecular hydrogel (**ZBM**) is formed after heating at 90 °C and subsequent cooling at room temperature for 5-10 minutes (Figure 1b) (see SI for detailed protocols). All the experiments discussed hereafter were performed at the same pH, concentration and ratio, unless otherwise mentioned. Interestingly, by exposing 1 mL of **ZBM** hydrogel to UV light (365 nm) for 15-20 minutes at room temperature, we observed a gel-to-sol transition (Figure 1b). Then, keeping the solution in the

dark for ~ 2 hours, the gel state was recovered, and this gel-sol-gel cycle could be repeated at least five times. In order to understand the phenomenon behind this reversible macroscopic behavior upon light irradiation, we first performed rheological measurements. For **ZBM** hydrogels made with **Z-FF** at concentrations comprised between 2 and 6 mg/mL (see SI), we determined their gel-sol transition temperatures by the simple vial inversion method. We used a heating block with a temperature increase of 2 °C / 10 minutes, and obtained the phase diagram represented in Figure 1c. Here, the gel-to-sol transition temperature of **ZBM** at a concentration of 5 mg/mL is observed at ~ 45 °C, whereas the gel at the same concentration melts at 20 °C under light irradiation. As a control experiment, we measured a temperature increase of only 2 °C during the UV irradiation of our sample using an IR camera (Figure S1), therefore excluding the hypothesis of a local photothermal effect leading to the observed melting transition at room temperature (Figure 1b). We also determined the phase diagrams of other possible combinations: **ZM**, **ZB** and **Z** hydrogels. **ZM** hydrogel (without **BPY** and using the same **Z-FF** concentration and molar ratio (4 **Z-FF**: 1 **MTA**)), **ZB** hydrogels (without motor and using the same **Z-FF** concentration and molar ratio (2 **Z-FF**: 1 **BPY**)), and of **Z** hydrogels (using concentrations comprised between 1 and 6 mg/mL of **Z-FF**) (Figure S2). These data show very similar trends for the four hydrogels, but with a systematic decrease in the melting temperatures upon increasing the number of components in the gel, suggesting that both the motor and the pyridine interact with the main gel structure formed by **Z-FF**. In order to understand the role of each subcomponent in the co-self-assembled hydrogel, **ZM**, **ZB** and **Z** hydrogels were analyzed together with **ZBM** using CD spectroscopy (Figures S6a, b, and c), and differences in the conformations of components were measured for each gel (see Figure S6 for more details). In particular, **MTA** showed strengthened interactions in the **ZBM** gel network compared to the **ZM** network. This illustrates the crucial role of **BPY** in bridging the **Z-FF** and **MTA** components in **ZBM**, in line with the role of **BPY** in gels made of **Z-FF** and bipyridine derivatives as already described in the literature.[31] To further study the mechanical behavior of **ZBM** hydrogels, a series of rheological experiments have been performed. First, we conducted a temperature ramp test with a sample loaded in its liquid state at 70 °C, and we recorded the shear moduli upon cooling (Figure S3). The sudden increase in shear moduli over a small temperature range (~ 5 °C) indicated a structural change in the sample, with the point of crossover between the storage (G') and loss (G") moduli at ~ 25 °C representing the point of gelation (sol-gel transition).[36,37] After the crossover point, G' increased by one order of magnitude higher than G" indicating the formation of a gel (soft solid-like material). Immediately after the sol-gel transition, an isothermal time sweep experiment was performed at 20 °C, to monitor the evolution of the shear moduli of the gel over time (Figure 1d). G' and G" increased overtime reaching a plateau after 2 hours, indicating that the gel has reached its stable network structure. To further determine the mechanical rigidity of the gel (*i.e.*, storage modulus), a dynamic frequency sweep experiment was performed over a 0.01 to 10 Hz frequency range (Figure 1e). The value of G' remained higher than that of G" across the frequency range investigated, and independent of the frequency in the hydrodynamic regime, thus indicating a solid-like behavior of the supramolecular gel with a shear elastic value of the physical network around 10 kPa.

2.2. Morphological characterization of motorized supramolecular hydrogels

The morphology of the gel was then examined by transmission electron microscopy (TEM) showing an entangled fibrous network (**Figure 2a**), with a polydisperse width of fiber in the range of ~ 100 nm (Figure S4a). In order to get further information on the local self-assembly of the observed fibers, the gel was analyzed by atomic force microscopy (AFM), suggesting the interesting formation of β-sheet secondary structures forming amyloid-like fibres[38] (Figure 2b,c and S4c). Indeed, the AFM section profile shows multi-layered flat ribbons with regular inter-sheet distances of 0.9 nm between two β-sheets, of 1.8 nm between three β-sheets, of 2.7 nm between four β-sheets, etc. (Figures 2d and S4d). These values are in agreement with the inter-sheet distances reported in literature for β-amyloid structures[39–41], and more particularly for those involving an antiparallel β-sheet arrangement (with a characteristic distance of 9.6 Å and less).[40,42] These microscopy data were well complemented with small angle X-ray scattering (SAXS) experiments which exhibit a characteristic q^{-2} dependence, also indicative of the presence of flat objects (Figures 2e). Comparing the experimental SAXS data with a numerical model of randomly oriented sheets yields an average thickness of 9.5 nm and an average width of 45 nm (see Figures S4e-g). To get further information on the local secondary structure, we performed solid-state FT-IR spectroscopy on **ZBM** xerogel, prepared by freeze-drying (see SI). Two bands of C=O stretching vibrations of the amide group, at 1690 and 1635 cm^{-1} are observed in the amide I region (Figure 2g), also characteristic of anti-parallel β-sheets[43–46], and with values that can be slightly shifted due to H/D exchange[47] as the gels were prepared in deuterated water. In order to have information on the percentage of anti-parallel organization of β-strands in the β-sheets, we used the β-sheet organizational index, *i.e.* the intensity ratio between the spectral bands ascribed to β-structure, 1695 and 1630 cm^{-1}, which is proportional to the percentage of anti-parallel arrangement of the β-strands in β-sheets.[48,49] High β-index values ranging between 0.2 and 0.3 have been reported as an evidence of anti-parallel β-strand arrangement in amyloid proteins[50,51], whereas it remains below 0.1 for parallel β-sheet proteins.[51] The calculated value of the β-sheet organizational index of **ZBM** xerogel based on the IR spectrum depicted in Figure 2g is ~ 0.3, a value high enough to confirm the presence of ~ 100% anti-parallel arrangement of β-strands.[49,50] Moreover, the secondary structures of **Z-FF** dipeptide have been particularly studied and reported to form amyloid-like fibers with an anti-parallel β-sheet conformation[52,53], whereas parallel and anti-parallel β-sheet branched structures can exist in co-self-assembled **Z-FF** / bipyridine hydrogels.[34] Based on these studies, we have prepared **ZB** and **Z** deuterated hydrogels using the same procedure, and recorded the FT-IR spectra on their xerogels (Figure S5a). **Z** xerogel showed very similar absorption bands to **ZBM** xerogel confirming approximately no change in the anti-parallel β-sheet secondary structure, whereas for **ZB** xerogel, the extra band at 1652 cm^{-1} showed the presence of unordered structures, turns or bends[46,54], as also confirmed by AFM image showing turns and twists (Figure S5b).

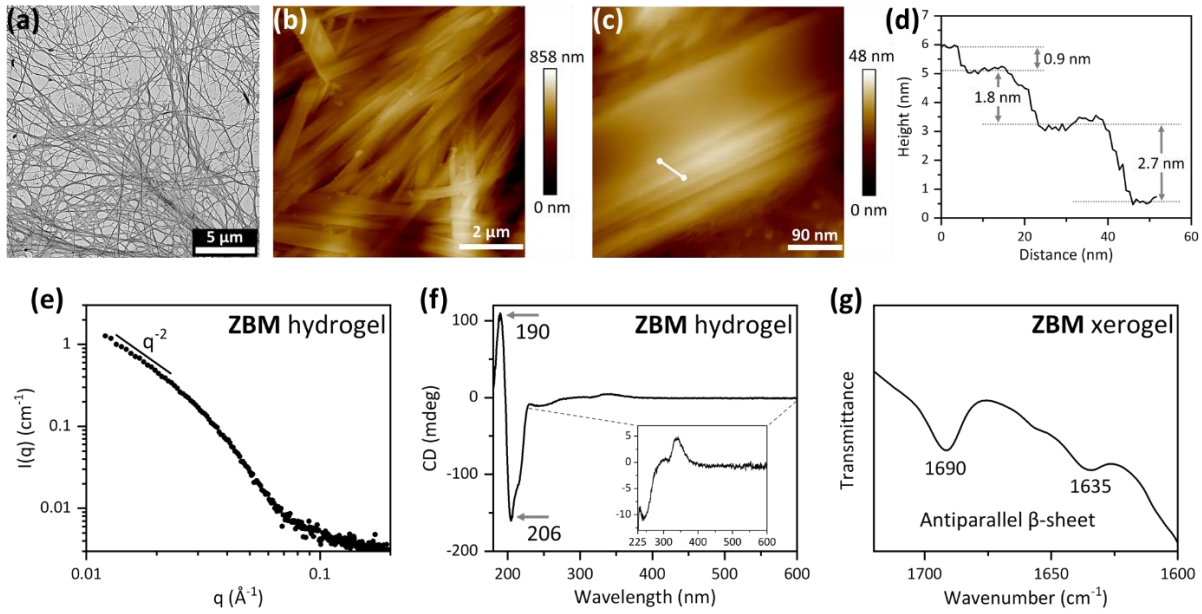

Figure 2. Structural characterizations of ZBM hydrogels. (**a**) TEM image of **ZBM** hydrogel (5 mg/mL of **Z-FF**, molar ratio 4: 4: 1). (**b-c**) Row AFM images of **ZBM** hydrogel showing amyloid fibers for two different magnifications (see Figure S4c for a corrected version of image 2c with levelling to supress distortion). (**d**) Typical height profile of amyloid fibers (section shown in **c**, white line). (**e**) Small-angle X-ray scattering and (**f**) circular dichroism spectrum of **ZBM** hydrogel. (**g**) Selected portion of the FT-IR spectrum of **ZBM** xerogel, characteristic of an anti-parallel β-sheet structure.

In addition, the circular dichroism (CD) spectrum in Figure 2f displays positive and negative Cotton effects at 190 and 206 nm respectively, indicating right-hand twisted anti-parallel β-sheets.[55,56] Compared to the CD spectrum of **Z** hydrogel at the same concentration, we noticed a blue shift of 3 nm (positive signal) and a red shift of 2 nm (negative signal) for **ZBM** hydrogel (193 nm and 204 nm, respectively in **Z** hydrogel) (Figure S6a), indicating the formation of a slightly modified molecular arrangement due to co-self-assembly.[34] Zooming on the 225-400 nm region in **ZBM** hydrogel, one can also satisfyingly see the expected signals of the **MTA** units with a positive (338 nm) and a negative (243 nm) Cotton effects. Comparing this signal to the CD spectrum of the **MTA** alone, we noticed a red shift of 3 nm in the positive signal and a blue shift of 20 nm in the negative signal (335 and 263 nm for **MTA** alone in solution) (Figure S6a), which is attributed to a slightly different conformation of the motor in the gel, thus giving a complementary evidence of its implication in the gel network.

In order to have a deeper insight into the intermolecular interactions involved in **ZBM** co-self-assembly, we performed FT-IR, ^{1}H NMR, and diffusion-ordered (DOSY) NMR spectroscopies. In the FTIR experiment (Figure S7), the bands at 1740 and 1700 cm^{-1} for **MTA**, and at 1707 cm^{-1} for **Z-FF** were attributed to the carboxylic acid C=O stretching, while for **BPY**, the band at 1588 cm^{-1} was ascribed to the C=N stretching. The disappearance of the C=O bands, the decrease in the intensity and broadening of the C=N band in **ZBM** xerogel, accompanied by the appearance of new bands in the amide I region (1690 and 1635 cm^{-1}), all indicate the presence of H-bonds between the three species in the co-self-assembled β-sheet structure (Figure S7a). In addition, at high frequencies (Figure S7b), the band at 3300 cm^{-1} was attributed

to the O-H (carboxylic acid) and N-H (amide) stretching in **Z-FF**, and the band at 2920 cm^{-1} corresponds to the O-H stretching of **MTA** carboxylic acid groups. The broadening of these bands in the co-self-assembled **ZBM** gel suggests also the participation of these functional groups in H-bonds. In addition, we performed DOSY on **ZBM** hydrogel and on the individual components **Z-FF**, **BPY** and **MTA** solutions (Figure S8). We noticed a decrease in the diffusion coefficient for all the individual components when co-assembled in **ZBM** hydrogel, supporting the presence of dynamic exchanges through intermolecular H-bonds among the three components,[57] in agreement with FT-IR observations. ^{1}H NMR spectra were also recorded for **ZBM** hydrogel and the individual components **Z-FF**, **BPY** and **MTA** solutions (Figure S9). All proton signals appear broader and less sharp in the gel indicating a change in the electronic environment of the protons as a result of intermolecular interactions.

2.3. Light-driven reversible gel-sol transitions of motorized supramolecular hydrogels

Strikingly, after motor actuation using UV light (365 nm, 365 $mW.cm^{-2}$) in **ZBM** hydrogel – which leads to the gel-sol transition (Figure 1b) – we observed by AFM and TEM the disruption of the large β-amyloid fibers into smaller assemblies (**Figures 3a,b** and S10a,b). Control experiments were then performed on **ZB** (without rotary motor) and on **ZBE** (with a non-rotating analog of **MTA** motor, in the form of its episulfide (**Epi-TA**), molar ratio 4 **Z-FF** : 4 **BPY** : 1 **Epi-TA**) hydrogels, having the same **Z-FF** concentration as **ZBM** hydrogel. By irradiating them under the same conditions (power and time), no gel-sol transition was observed at the macroscopic scale, and the integrity of the local structure was also confirmed by looking at the hydrogels by STEM and AFM (Figures S11d,d' and g,g'). At that stage, we performed ^{1}H NMR experiments both during irradiation of the gel state and immediately after light irradiation in the sol (Figure S12), and we did not observe any isomerization of the motor to its unstable helical state. The absence of unstable helix was supported by UV-Vis measurements done also before and after UV irradiation (Figure S13a), showing no significant change in the spectrum, and mainly no appearance of new absorption bands.[58,59] The same conclusion was drawn based on CD experiments recorded before and after UV irradiation (Figure 3f), showing no signal inversion, confirming again that the unstable helix was not kinetically trapped.[58,60] Therefore, all these experiments demonstrate that the influence of the motor on disrupting the β-amyloid fibers is the result of its relatively fast rotation, and not of its isomerization state (*i.e.* between its stable and its unstable helical forms). After motor actuation, the **ZBM** solution was left in the dark for 3 days (showing the recovery of a self-supporting hydrogel after only two hours) (Figure 1b). Satisfyingly, both AFM and TEM micrographs revealed full recovery of the gel network made of the initially observed large β-amyloid fibers (Figures 3c and S10c). As expected, the ^{1}H NMR shifted signals also recovered in the dark, to reach approximately their initial position in the gel for **MTA**, indicating the recovery of the supramolecular interactions in the gel network (Figure S12b).

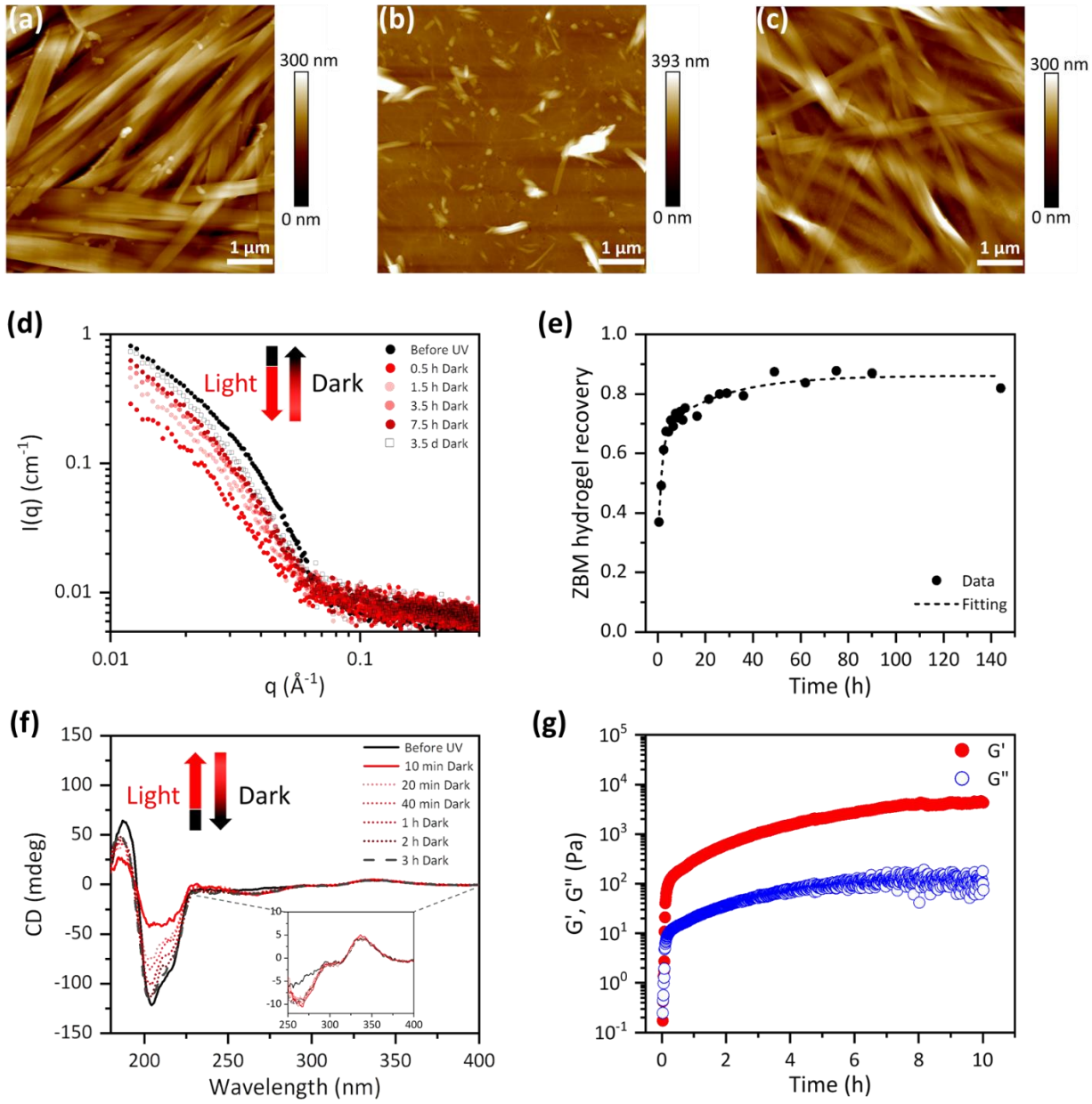

Figure 3. Dynamic characterizations of the ZBM sol-gel transition. (**a-c**) AFM images of **ZBM** hydrogel before UV irradiation (**a**); after 20 minutes of UV irradiation showing the breakage of the β-amyloid fibers (**b**), and after their recovery in the dark for 3 days (**c**), respectively. (**d**) Evolution of SAXS profiles after UV irradiation (3 min for 30 µL of gel) and in the dark for 3 days, showing the recovery of the initial local structure of the gel. (**e**) Recovery of **ZBM** hydrogel structure extracted from SAXS measurements. (**f**) Evolution of the CD spectra after UV irradiation (3 min for 30 µL of gel) and in the dark for 3 hours, showing the recovery of the β-sheets. (**g**) Evolution of the shear moduli over time after UV irradiation, and recovery of the gel mechanical strength from the sol state (t = 0 minutes is the time when UV irradiation was stopped).

The light-triggered gel-sol transition and the recovery in the dark was also probed by SAXS. The **ZBM** gel was measured before irradiation (Figure 3d, black), and after irradiation (but with a 30-minute delay in the dark, that is the time necessary for the measurement). A noticeable decrease of almost one decade in the scattered intensity occurred, supporting the macroscopic and microscopic observation of the fibers' disruption after UV irradiation. Following the

evolution of the system as a function of time in the dark, the structure recovered in more than 60% after around 8 hours, and evolved slower to recover approximately 90 % after 3 days (Figure 3d,e). The β-sheet secondary structure in **ZBM** hydrogel was also studied using CD before (Figure 3f, black) and after UV irradiation for 3 minutes, until a sol state is achieved (Figure 3f, red line – 10 minutes dark). The intensities of both negative 206 nm and positive 190 nm signals decreased to more than a half of their initial intensities during light irradiation, supporting TEM, AFM and SAXS experiments in the disruption of β-sheets. The structure recovery was followed in the dark, with a time of 20 minutes being necessary to recover approximately 50% of the structure, followed by a slower evolution to recover most of the β-sheet secondary structures after 3 hours. Finally, the mechanical properties of the gel were measured after UV irradiation. Immediately after gel-sol transition under UV irradiation, the solution was loaded into the rheometer to record the evolution of moduli as a function of time (Figure 3g). G' and G" increased sharply and immediately after stopping UV, with G' higher than G", indicating that the gel structure starts to recover immediately after stopping light irradiation. Nevertheless, 10 hours were needed to recover and stabilize the original mechanical properties of the gel, indicating a slower kinetics of recovery after the disruption of the gel network by UV light, compared to its disruption by heating (Figure 1d). This can be correlated with the observation that the disruption of the network by light resulted in small dispersed assemblies in solution, as characterized by AFM, TEM, and SAXS, which agrees with the breakage of supramolecular interactions only where the rotating motors are involved in the co-self-assembly. On the other hand, disruption of the gel network by heating results in homogeneous breakage of all supramolecular interactions as homogeneous unimers form in solution. Therefore, it is evident that recovering the network from unimers in solution compared to existing small assemblies shows different gelation time regimes due to different possible mechanisms. This illustrates the unique effect of the motor rotation and of the generated torque on the network disruption, confirming that the gel-sol transition is the result of the constant mechanical work produced by the molecular motor. After the time sweep experiment, the storage modulus was determined by a dynamic frequency sweep experiment. This experiment did not last more than 10 hours after stopping the light in order to avoid any wrong measurements that could result from water evaporation (Figure S14). Nevertheless, after this time, G' reached a value close to the initial one (10 kPa), and remained greater than G" across the entire frequency range recorded.

Based on macroscopic observations, rheological measurements, microscopic imaging, and spectroscopic data, we propose a simplified representation of the motorized **ZBM** hydrogel system in **Figure 4** (see also Figure S15 summarizing key control experiments that support the proposed mechanism). This system forms anti-parallel β-amyloid-like fibers at thermodynamic equilibrium by co-self-assembly of **Z-FF**, **BPY** and **MTA**. The schematic representation of the **ZBM** hydrogel at thermodynamic equilibrium depicts the interaction of **Z-FF** acid moieties with **BPY** through H-bonding, and the integration of the **MTA** in the network through H-bonding interactions of the four acid moieties with **BPY**. Therefore, **BPY** acts as a linker between **MTA** and **Z-FF** in the network.

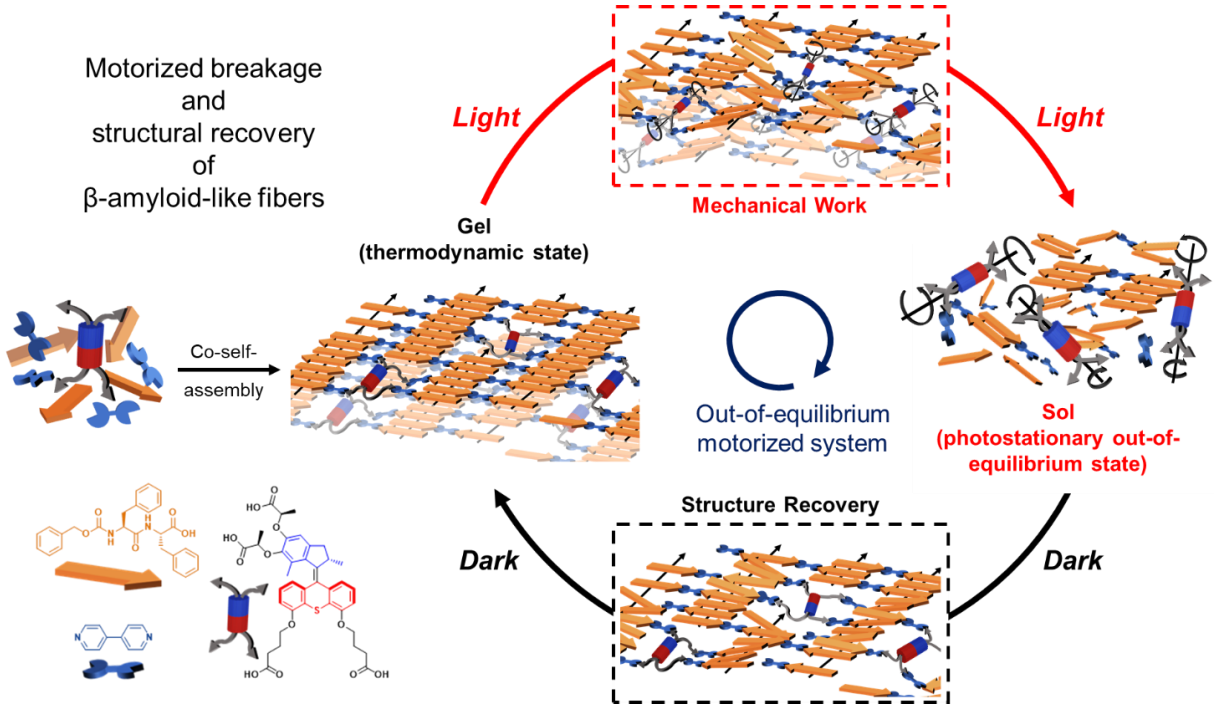

Figure 4. Schematic representation of the out-of-equilibrium motorized system based on ZBM hydrogels. Under UV irradiation, the co-self-assembly of β-amyloid fibers formed at thermodynamic equilibrium is broken by the work produced during the motor rotation, and the system reaches a photostationary state in the sol. Conversely, when the rotation of the molecular motor is stopped in the dark, the thermodynamically stable β-amyloid structure is recovered.

When exposed to UV irradiation, the unidirectional rotation of molecular motors is activated, producing nanomechanical work in the gel network. This motion subsequently drives the disruption of the β-amyloid fibers by breaking supramolecular interactions between the co-self-assembled entities. Finally, disruption of the fibers disconnects the gel network, resulting in an out-of-equilibrium gel-to-sol transition at the photostationary state. In order to control the impact of **BPY** in our supramolecular design under UV light, we prepared **ZM** hydrogel (without **BPY** and using the same **Z-FF** concentration and molar ratio (4 **Z-FF**: 1 **MTA**)) and exposed it to the same irradiation conditions. However, no changes were observed in the macroscopic gel behavior, nor in the integrity of the gel network at the microscopic scale when examined by STEM (Figures S11e,e'). Analysing **ZM** hydrogel by CD spectroscopy also revealed minimum interactions in the network compared to **ZBM** (see Figure S6c for more details). These observations suggest that the delicate design of the **ZBM** hydrogel system comprising **BPY** is necessary to achieve gel-to-sol transition under UV light, by bridging the **Z-FF** and **MTA** units through hydrogen bonds. Moreover, we were interested in investigating the importance of having four carboxylic acid arms on the motor (**MTA**) connected to the gel network. Therefore, we functionalized the same motor core with only two carboxylic acids on its upper part (motor di-acid, **MDA**) (see SI for synthetic protocol and product characterization). We prepared **ZBMDA** hydrogel (integrating **MDA** instead of **MTA** and using the same **Z-FF** concentration with a molar ratio 2 **Z-FF**: 2 **BPY**: 1 **MTA**) (Figure S6e). **MDA** can interact with the gel network through its two acid moieties, but is in principle unable to generate a torque on the gel network during its rotation. When exposing **ZBMDA** gel to UV light in the same conditions, no macroscopic nor microscopic changes were observed (Figures S11f,f').

Therefore, as expected, **MDA** turns freely on its rotor part, without disrupting the gel network. Interestingly, this confirms that the production of work necessary to disrupt the network upon **MTA** rotation results from the force of the torque which requires a four-arm connection to the network. After reaching the photostationary state in **ZBM** system, stopping UV irradiation and keeping the solution in the dark, molecular motors stop producing work on the system, allowing the β-sheet to reform by re-establishing their supramolecular H-bonds, and ultimately resulting in the recovery of the thermodynamically stable β-amyloid fibers. It is therefore a very different mechanism compared to those involved in previously reported systems where gel-sol[59], sol-gel[20,61], or gel-gel[62] transitions were achieved by switching a (photo)-responsive molecule from one conformation to another, and therefore changing the nature of the self-assembly as a function of its isomerization state.

3. Conclusion

In summary, we have designed a co-self-assembled supramolecular hydrogel system that integrates light-driven molecular motors together with β-amyloid-like fibers. We have demonstrated the possibility of achieving reversible gel-sol-gel transitions by implementing the mechanical work produced by the collective rotation of molecular motors in the supramolecular network under UV light irradiation, through the endergonic breakage of β-amyloid fibers. The efficiency of the motor rotation is particularly evident in doing this work, because it allows melting of the present hydrogel at 20 °C, while its purely thermally activated phase transition would occur only at a temperature of 45 °C. It is important to point out that this mechanical actuation is independent of the isomerization state of the motor, with a population that stays on average in its stable helix conformation, but relies only on the transitory rotation that takes place during light irradiation. This event can also be interpreted as the result of a change in the apparent stability constant of the co-self-assembly under motor rotation, which generates a disrupting torque on the supramolecular network. This represents, to the best of our knowledge, the first example revealing the potential of autonomous molecular motors for driving the out-of-equilibrium reconfiguration of supramolecular polymers and supramolecular polymer networks. It illustrates the high potential of such molecular motors by exploiting their continuous unidirectional motion and their cumulative production of mechanical work. The fact that this first example involves diphenylalanine fibers which are good models of β-amyloid polypeptides[63] makes it particularly interesting, considering the importance of such structures in biology and medicine.[64,65] We believe that this kind of approach in materials science, using artificial molecular motors to transduce various kinds of energy sources in mechanical work, is of particular interest in order to design an entirely new kind of responsive materials capable of working in out-of-equilibrium thermodynamic conditions such as those encountered in living systems.[23]

Supporting Information

Synthetic protocols and characterization of synthesized compounds; their corresponding ^{1}H and ^{13}CNMR spectra; hydrogels and xerogels preparation procedure; irradiation experiments supplementary data on gels phase-diagram, additional FT-IR, ^{1}H NMR, DOSY, CD, UV-Vis, TEM, AFM, SAXS, and rheology experiments.

Acknowledgements

This work was granted by the European Commission's Horizon 2020 Programme as part of the MSCA-ITN project ArtMoMa under grant no. 860434. The authors wish to acknowledge the Centre National de la Recherche Scientifique (CNRS), the University of Strasbourg, and the Fondation Jean-Marie Lehn. They thank SOLEIL for the provision of synchrotron radiation facilities and Thomas Bizien for assistance in using beamline SWING for the SAXS and WAXS experiments. They also thank the DiffériX platform of the Institut Charles Sadron for in-house SAXS measurements.

References

[1] V. Balzani, A. Credi, F. M. Raymo, J. F. Stoddart, *Angew. Chem. Int. Ed.* **2000**, *39*, 3348.

[2] K. Kinbara, T. Aida, *Chem. Rev.* **2005**, *105*, 1377.

[3] W. R. Browne, B. L. Feringa, *Nat. Nanotechnol.* **2006**, *1*, 25.

[4] J.-P. Sauvage, *Angew. Chem. Int. Ed.* **2017**, *56*, 11080.

[5] F. Lancia, A. Ryabchun, N. Katsonis, *Nat. Rev. Chem.* **2019**, *3*, 536.

[6] S. Corra, M. Curcio, M. Baroncini, S. Silvi, A. Credi, *Adv. Mater.* **2020**, *32*, 1906064.

[7] A. Mondal, R. Toyoda, R. Costil, B. L. Feringa, *Angew. Chem. Int. Ed.* **2022**, *61*, e2022066.

[8] D. Dattler, G. Fuks, J. Heiser, E. Moulin, A. Perrot, X. Yao, N. Giuseppone, *Chem. Rev.* **2020**, *120*, 310.

[9] A. Perrot, E. Moulin, N. Giuseppone, *Trends Chem.* **2021**, *3*, 926.

[10] G. Ragazzon, M. Baroncini, S. Silvi, M. Venturi, A. Credi, *Nat. Nanotechnol.* **2015**, *10*, 70.

[11] C. Pezzato, C. Cheng, J. F. Stoddart, R. D. Astumian, *Chem. Soc. Rev.* **2017**, *46*, 5491.

[12] S. Kassem, T. van Leeuwen, A. S. Lubbe, M. R. Wilson, B. L. Feringa, D. A. Leigh, *Chem. Soc. Rev.* **2017**, *46*, 2592.

[13] Y. Feng, M. Ovalle, J. S. W. Seale, C. K. Lee, D. J. Kim, R. D. Astumian, J. F. Stoddart, *J. Am. Chem. Soc.* **2021**, *143*, 5569.

[14] S. Corra, M. T. Bakić, J. Groppi, M. Baroncini, S. Silvi, E. Penocchio, M. Esposito, A. Credi, *Nat. Nanotechnol.* **2022**, *17*, 746.

[15] C. J. Bruns, J. F. Stoddart, *The Nature of the Mechanical Bond*, John Wiley & Sons, Inc., Hoboken, NJ, USA, **2016**.

[16] J. Chen, F. K.-C. Leung, M. C. A. Stuart, T. Kajitani, T. Fukushima, E. van der Giessen, B. L. Feringa, *Nat. Chem.* **2018**, *10*, 132.

[17] E. Moulin, C. C. Carmona-Vargas, N. Giuseppone, *Chem. Soc. Rev.* **2023**, *52*, 7333.

[18] J. Hou, A. Mondal, G. Long, L. Haan, W. Zhao, G. Zhou, D. Liu, D. J. Broer, J. Chen, B. L. Feringa, *Angew. Chem. Int. Ed.* **2021**, *60*, 8251.

[19] J. Li, S. Xie, J. Meng, Y. Liu, Q. Zhan, Y. Zhang, L. Shui, G. Zhou, B. L. Feringa, J. Chen, *CCS Chem.* **2023**, DOI: 10.31635/ccschem.023.202303171.

[20] Y. Shan, Q. Zhang, J. Sheng, M. C. A. Stuart, D. Qu, B. L. Feringa, *Angew. Chem. Int. Ed.* **2023**, *62*, e202310582.

[21] E. Moulin, L. Faour, C. C. Carmona-Vargas, N. Giuseppone, *Adv. Mater.* **2020**, *32*, 1906036.

[22] A. Perrot, W. Wang, E. Buhler, E. Moulin, N. Giuseppone, *Angew. Chem. Int. Ed.* **2023**, *62*, e202300263.

[23] N. Giuseppone, A. Walther, Eds., *Out-of-Equilibrium (Supra)Molecular Systems and Materials*, John Wiley And Sons, **2021**.

[24] N. Koumura, R. W. J. Zijlstra, R. A. van Delden, N. Harada, B. L. Feringa, *Nature* **1999**, *401*, 152.

[25] C. Gao, A. Vargas Jentzsch, E. Moulin, N. Giuseppone, *J. Am. Chem. Soc.* **2022**, *144*, 9845.

[26] R. Wilcken, M. Schildhauer, F. Rott, L. A. Huber, M. Guentner, S. Thumser, K. Hoffmann, S. Oesterling, R. de Vivie-Riedle, E. Riedle, H. Dube, *J. Am. Chem. Soc.* **2018**, *140*, 5311.

[27] Q. Li, G. Fuks, E. Moulin, M. Maaloum, M. Rawiso, I. Kulic, J. T. Foy, N. Giuseppone, *Nat. Nanotechnol.* **2015**, *10*, 161.

[28] J. T. Foy, Q. Li, A. Goujon, J.-R. Colard-Itté, G. Fuks, E. Moulin, O. Schiffmann, D. Dattler, D. P. Funeriu, N. Giuseppone, *Nat. Nanotechnol.* **2017**, *12*, 540.

[29] A. Mukherjee, G. R. Desiraju, *Chem. Commun.* **2011**, *47*, 4090.

[30] T. R. Shattock, K. K. Arora, P. Vishweshwar, M. J. Zaworotko, *Cryst. Growth Des.* **2008**, *8*, 4533.

[31] G. F. Liu, L. Y. Zhu, W. Ji, C. L. Feng, Z. X. Wei, *Angew. Chem. Int. Ed.* **2016**, *55*, 2411.

[32] G. Liu, J. Sheng, H. Wu, C. Yang, G. Yang, Y. Li, R. Ganguly, L. Zhu, Y. Zhao, *J. Am. Chem. Soc.* **2018**, *140*, 6467.

[33] F. Wang, C. L. Feng, *Chem. Eur. J.* **2018**, *24*, 1509.

[34] W. Ji, Y. Tang, P. Makam, Y. Yao, R. Jiao, K. Cai, G. Wei, E. Gazit, *J. Am. Chem. Soc.* **2021**, *143*, 17633.

[35] W. Ji, C. Yuan, P. Chakraborty, S. Gilead, X. Yan, E. Gazit, *Commun. Chem.* **2019**, *2*, 65.

[36] G. Stojkov, Z. Niyazov, F. Picchioni, R. K. Bose, *Gels* **2021**, *7*, 255.

[37] P. L. Drzal, K. R. Shull, *Macromolecules* **2003**, *36*, 2000.

[38] D. S. Eisenberg, M. R. Sawaya, *Annu. Rev. Biochem.* **2017**, *86*, 69.

[39] W. T. Astbury, S. Dickinson, K. Bailey, *Biochem. J.* **1935**, *29*, 2351.

[40] M. Sunde, C. Blake, *Adv. Protein Chem.* **1997**, *50*, 123.

[41] J. Greenwald, R. Riek, *Structure* **2010**, *18*, 1244.

[42] S. J. Roeters, A. Iyer, G. Pletikapiä, V. Kogan, V. Subramaniam, S. Woutersen, *Sci. Rep.* **2017**, *7*, 1.

[43] T. Miyazawa, E. R. Blout, *J. Am. Chem. Soc.* **1961**, *83*, 712.

[44] P. I. Haris, D. Chapman, *Biopolymers* **1995**, *37*, 251.

[45] W. Dzwolak, V. Smirnovas, *Biophys. Chem.* **2005**, *115*, 49.

[46] A. Barth, *Biochim. Biophys. Acta - Bioenerg.* **2007**, *1767*, 1073.

[47] E. Goormaghtigh, V. Cabiaux, J. M. Ruysschaert, *Subcell. Biochem.* **1994**, *23*, 363.

[48] Y. N. Chirgadze, N. A. Nevskaya, *Biopolymers* **1976**, *15*, 627.

[49] R. Sarroukh, E. Goormaghtigh, J. Ruysschaert, V. Raussens, *Biochim. Biophys. Acta* **2013**, *1828*, 2328.

[50] E. Cerf, R. Sarroukh, S. Tamamizu-Kato, L. Breydo, S. Derclayes, Y. F. Dufrênes, V. Narayanaswami, E. Goormaghtigh, J. M. Ruysschaert, V. Raussens, *Biochem. J.* **2009**, *421*, 415.

[51] M. S. Celej, R. Sarroukh, E. Goormaghtigh, G. D. Fidelio, J. M. Ruysschaert, V. Raussens, *Biochem. J.* **2012**, *443*, 719.

[52] M. Reches, E. Gazit, *Isr. J. Chem.* **2005**, *45*, 363.

[53] N. Brown, J. Lei, C. Zhan, L. J. W. Shimon, L. Adler-Abramovich, G. Wei, E. Gazit, *ACS Nano* **2018**, *12*, 3253.

[54] J. Kubelka, T. A. Keiderling, *J. Am. Chem. Soc.* **2001**, *123*, 12048.

[55] C. A. Bush, S. K. Sarkar, K. D. Kopple, *Biochemistry* **1978**, *17*, 4951.

[56] A. Micsonai, F. Wien, L. Kernya, Y. H. Lee, Y. Goto, M. Réfrégiers, J. Kardos, *Proc. Natl. Acad. Sci. U. S. A.* **2015**, *112*, E3095.

[57] S. R. Chaudhari, N. Suryaprakash, *J. Mol. Struct.* **2012**, *1016*, 163.

[58] A. Ryabchun, F. Lancia, J. Chen, D. Morozov, B. L. Feringa, N. Katsonis, *Adv. Mater.* **2020**, *32*, 2004420.

[59] S. J. Wezenberg, C. M. Croisetu, M. C. A. Stuart, B. L. Feringa, *Chem. Sci.* **2016**, *7*, 4341.

[60] R. A. van Delden, M. K. J. ter Wiel, M. M. Pollard, J. Vicario, N. Koumura, B. L. Feringa, *Nature* **2005**, *437*, 1337.

[61] Z. Gao, F. Yan, L. Shi, Y. Han, S. Qiu, J. Zhang, F. Wang, S. Wu, W. Tian, *Chem. Sci.* **2022**, *13*, 7892.

[62] Y. Qin, Y. Wang, J. Xiong, Q. Li, M. - H. Zeng, *Small* **2023**, *19*, 2207785.

[63] S. Brahmachari, Z. A. Arnon, A. Frydman-Marom, E. Gazit, L. Adler-Abramovich, *ACS Nano* **2017**, *11*, 5960.

[64] M. G. Iadanza, M. P. Jackson, E. W. Hewitt, N. A. Ranson, S. E. Radford, *Nat. Rev. Mol. Cell Biol.* **2018**, *19*, 755.

[65] T. P. J. Knowles, M. Vendruscolo, C. M. Dobson, *Nat. Rev. Mol. Cell Biol.* **2014**, *15*, 384.

Graphical abstract for TOC

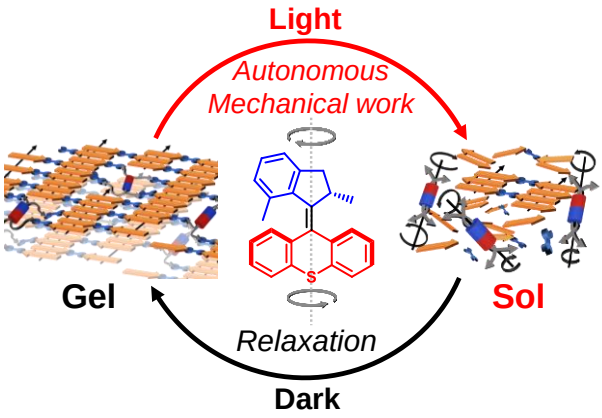

A light-driven rotary motor is co-self-assembled in a β-amyloid-like structure forming supramolecular hydrogels. Upon UV irradiation, the work produced by the continuous rotation of the motor is shown to disrupt the hydrogen bonds of the self-assembled system, leading to an endergonic gel-to-sol transition in out-of-equilibrium conditions. The structure of the original hydrogel is subsequently recovered in the dark.